Supporting Information

A Multifunctional Nanocatalytic Ferroptosis Amplifier Based on Glutathione Scavenging and Lipid Peroxidation Amplification for Cancer Therapy

Yafei Lin‡[a], Xue Han‡[a], Lei Wang[a], Zhuoran Li[a], Wenting Zhang[a], Xuening Zhang[a], Yueyang Yao[a], Yonghao Gai*[a], Xi Zhu*[b], Yang Zhang*[a]

[a]Department of Ultrasound, Shandong Provincial Hospital Affiliated to Shandong First Medical University, Jinan, Shandong, 250021, P.R. China. E-mail: ultra_gaiyonghao@163.com; wonderfulwater1989@163.com

[b]Institute of Biomedical Engineering, Kunming Medical University, Kunming, Yunnan, 650500, P.R. China. E-mail: zhuxi@kmmu.edu.cn

‡ The authors contribute equally to this article.

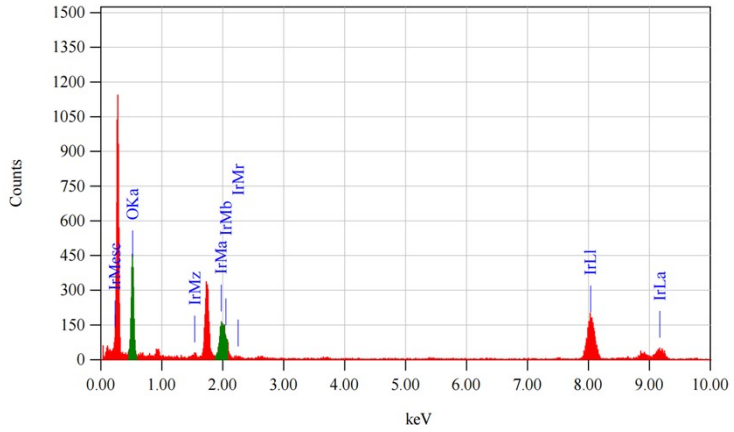

Fig. S1 EDS of IrO_x nanoparticles.

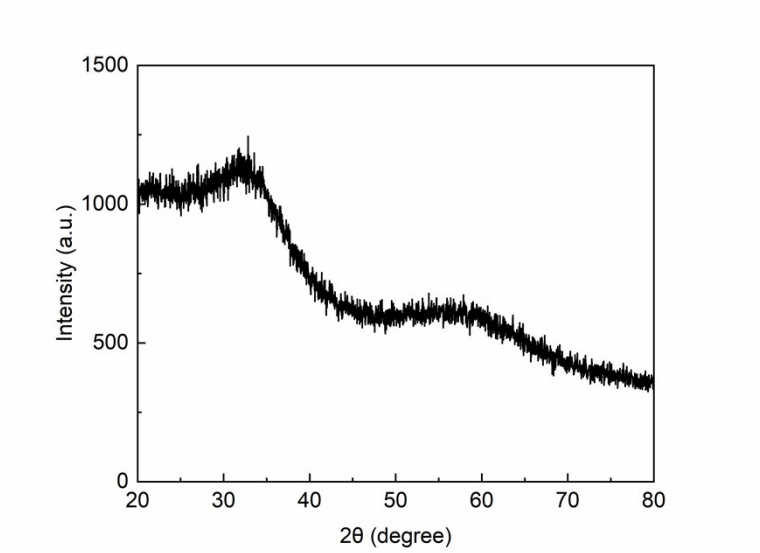

Fig. S2 XRD spectrum of IrO_x nanoparticles.

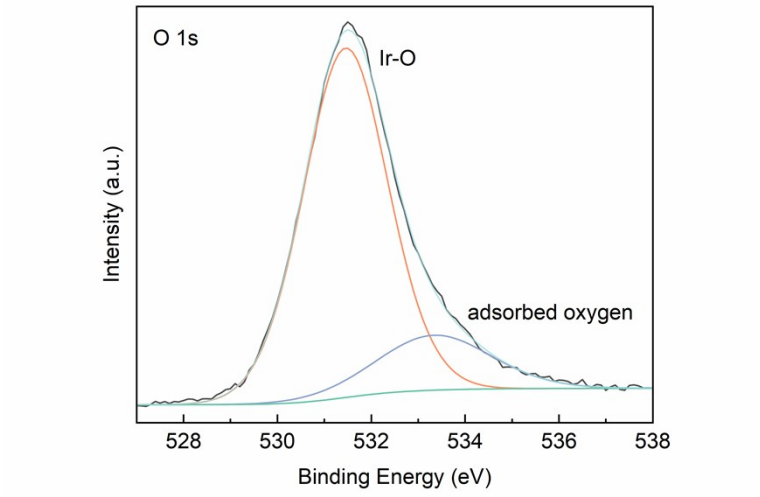

Fig. S3 O 1s XPS spectrum of the IrO_x nanoparticles.

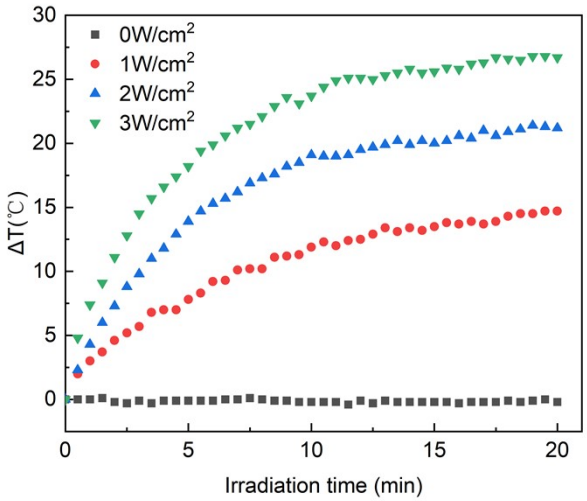

Fig. S4 The curve shows the temperature change of IrO_x@HMME-HSA aqueous solutions with a concentration of 100μg/mL over 20 min irradiation of different power densities (0, 1, 2, and 3 W/cm²).

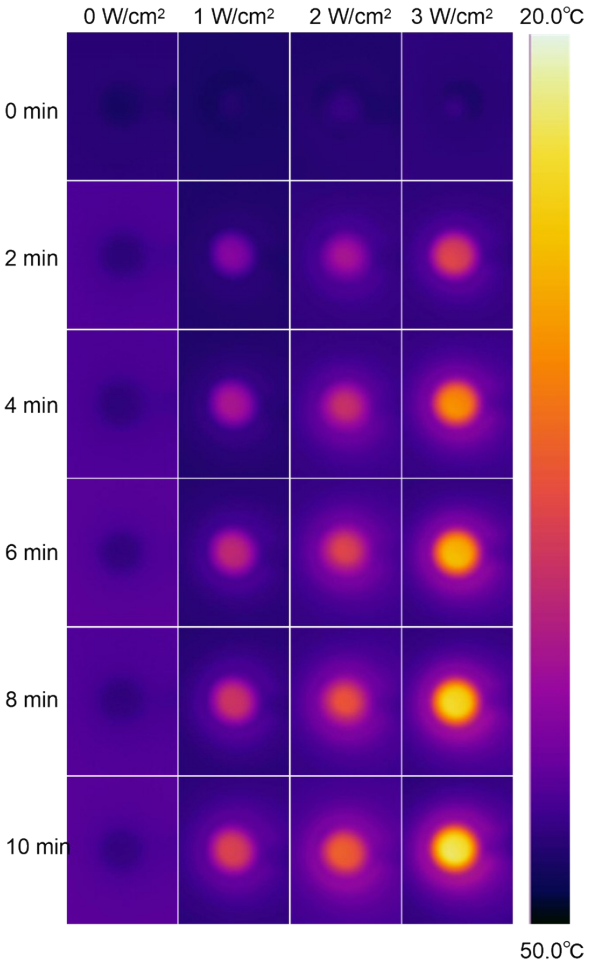

Fig. S5 Thermal image of the IrO_x@HMME-HSA aqueous solution under laser irradiation of different power densities (0, 1, 2, and 3 W/cm²).

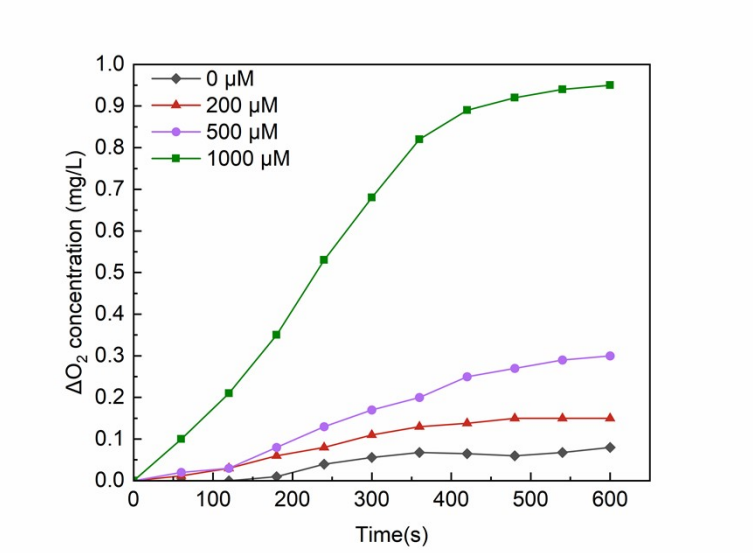

Fig. S6 The curves show the O_2 production of IrO_x@HMME-HSA solutions at different concentrations of H_2O_2 (0, 200, 500, 1000μM).

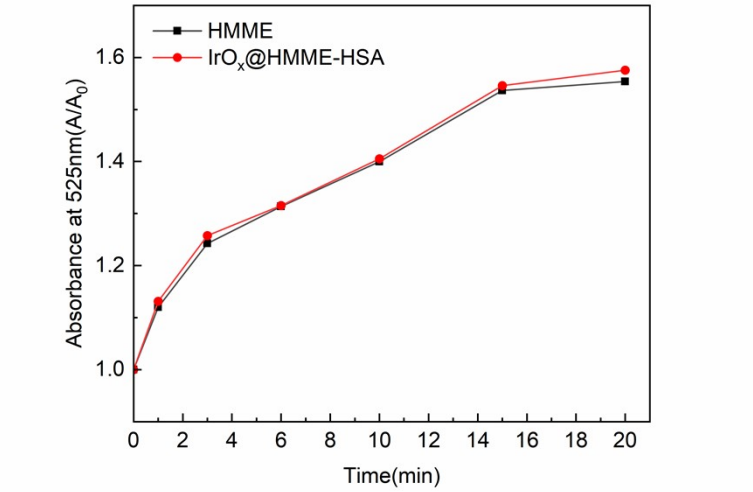

Fig. S7 Time-dependent generation of singlet oxygen ($^1O_2$) detected using SOSG as a probe. The fluorescence intensity of the reaction product at 525 nm (A/A_0) was monitored over time for HMME and IrO_x@HMME-HSA.

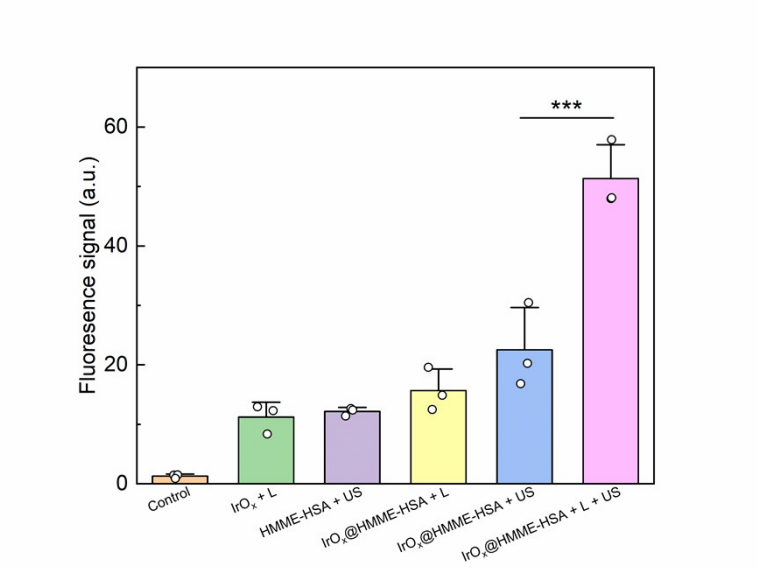

Fig. S8 Semi-quantitative analysis of ROS-related fluorescence intensity in Fig. S3C by Image J software. Data are presented as the mean ± SD (n = 3). Significant differences were assessed using t test (***$p < 0.001$).

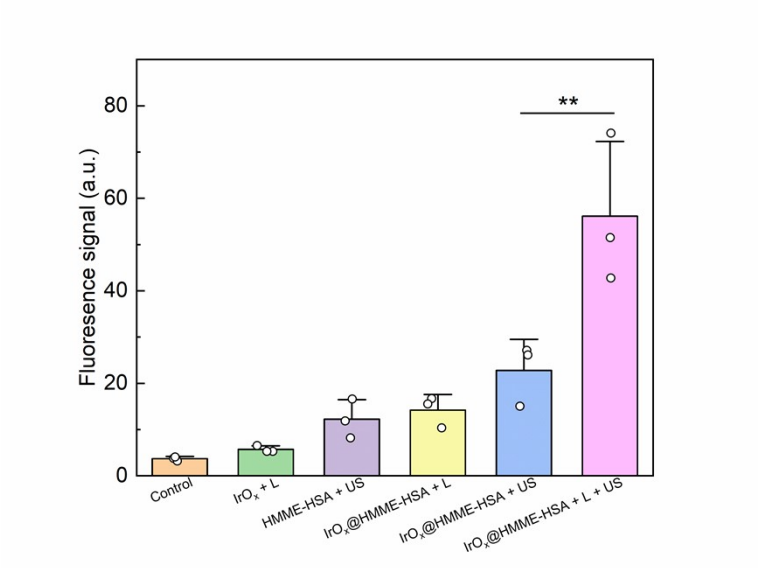

Fig. S9 Semi-quantitative analysis of LPO fluorescence intensity. Data are represented as mean ± SD (n = 3;**$p < 0.01$).

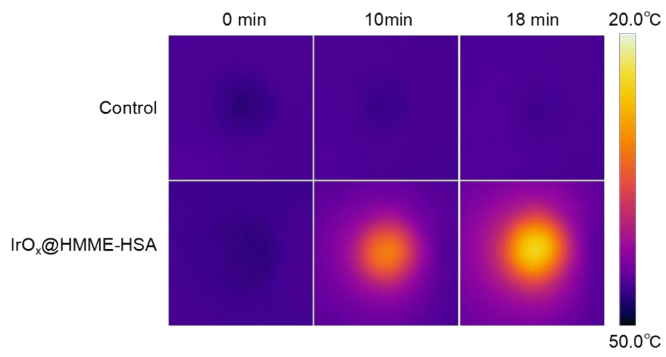

Fig. S10 Time-course thermal images of the change in solution temperature culture dishes containing PC-3cells subjected to laser irradiation.

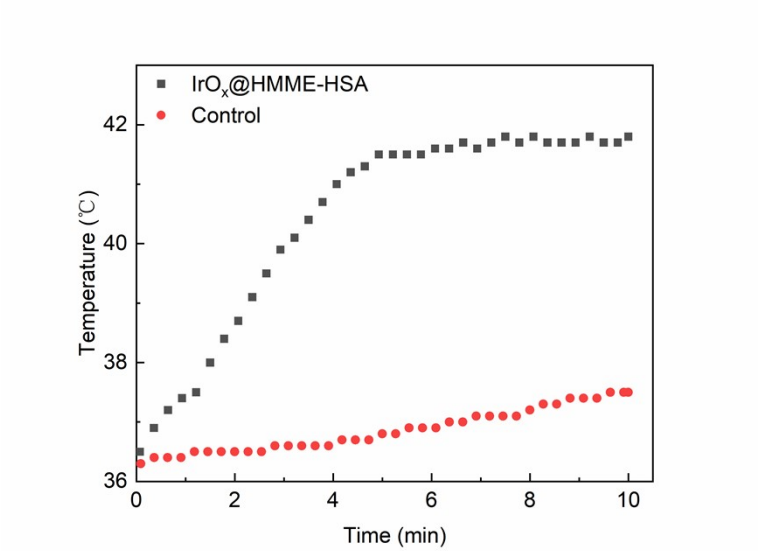

Fig. S11 Curves shows the temperature change in the body surface of the nude mice under laser irradiation, as recorded using a thermal infrared camera.

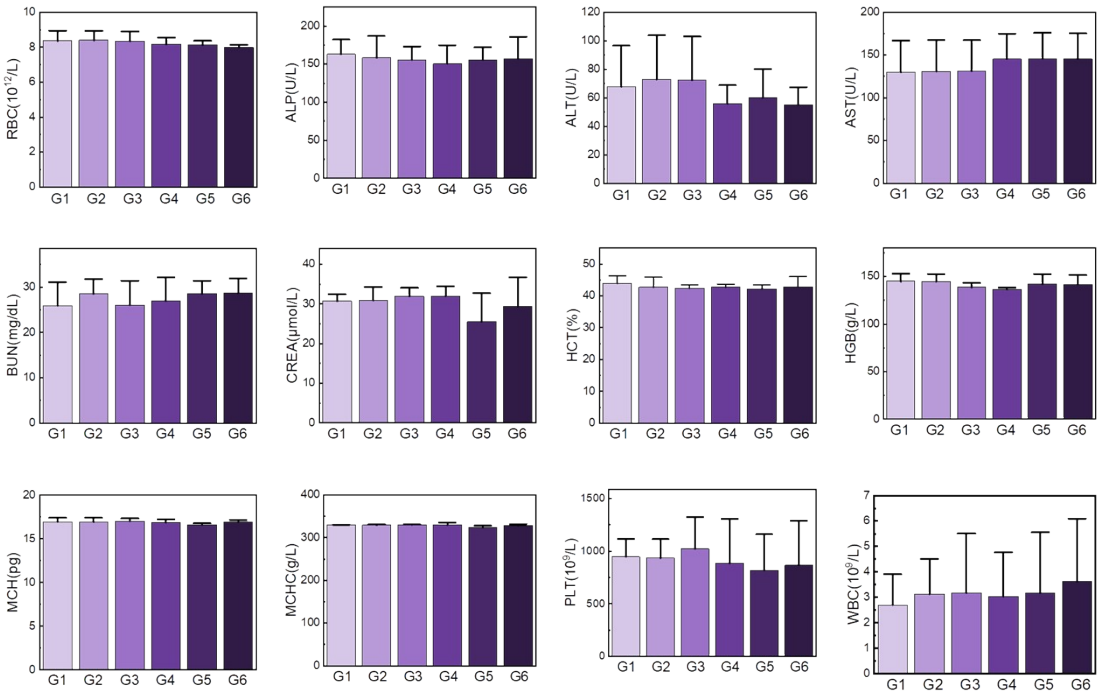

Fig. S12 Hematological tests, such as regular blood indicators(WBC, PLT, RBC, HCT, MCH, MCHC, HGB,) and functions of liver and kidney (ALT, AST, ALP, CREA, BUN) of different groups (G1: Control, G2: IrO_x + L, G3: HMME-HSA + US, G4: IrO_x@HMME-HSA + L, G5: IrO_x@HMME-HSA + US, G6: IrO_x@HMME-HSA

+ L + US) on day 21 after various treatments. The date are expressed as means ± SD (n = 3) (***$p < 0.001$, **$p < 0.01$, and *$p < 0.05$).

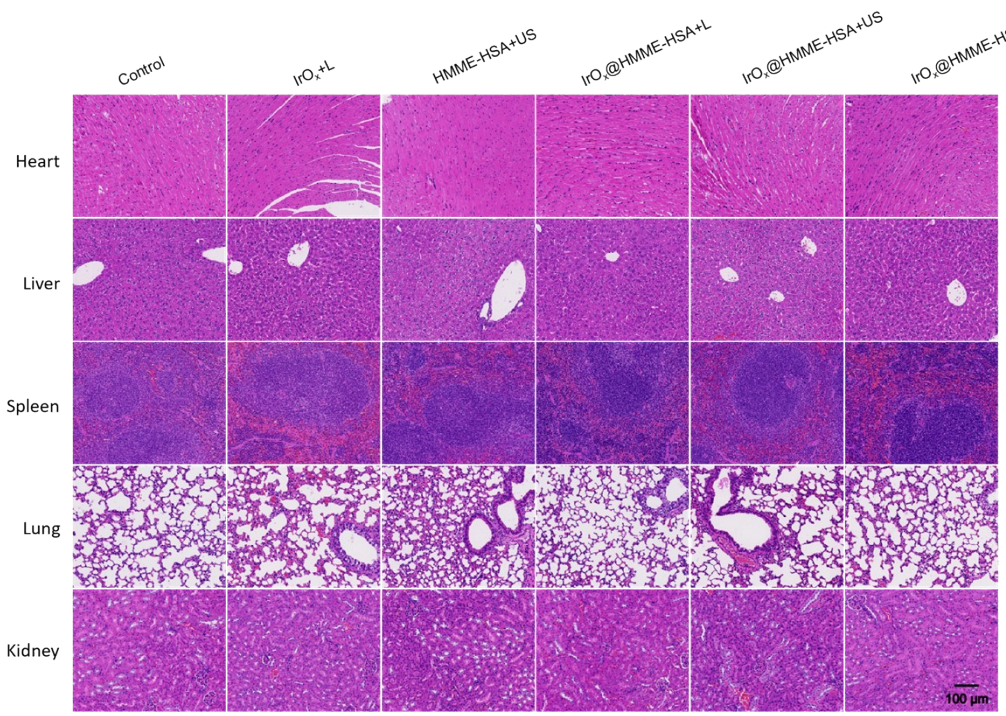

Fig. S13 Images of H&E-stained sections of the heart, liver, spleen, lung and kidney from mice in each treatment group , scale bar = 100 μm.

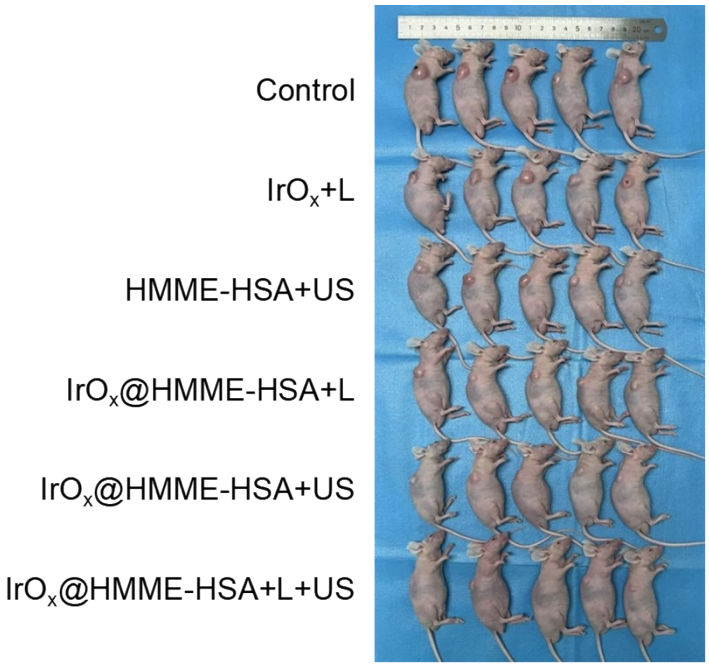

Fig. S14 Representative images of tumor-bearing nude mice of different groups.

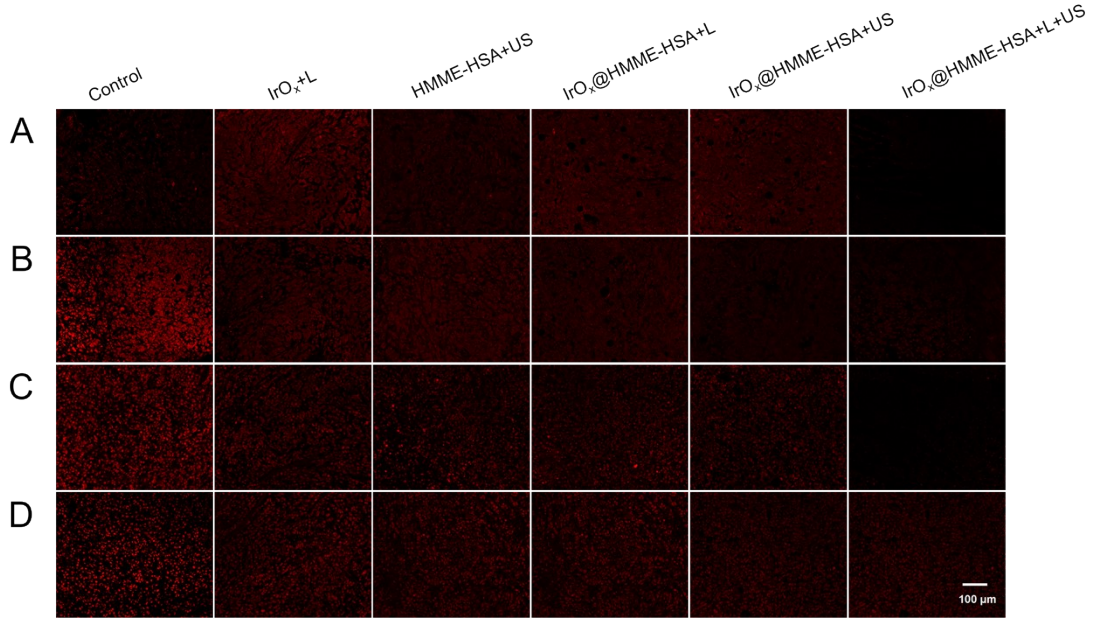

Fig. S15 Fluorescence images of tumor slices after HSP70 (A), SLC7A11 (B), GCLM (C), and HIF-1α (D) immunofluorescence staining ,scale bar = 100 μm.